

A Theoretical Study of the Signal Contribution of Regions of the Adult Head to Near-Infrared Spectroscopy Studies of Visual Evoked Responses

Michael Firbank, Eiji Okada,* and David T. Delpy†,1

University Department of Radiology, Imaging Laboratory, Royal Victoria Infirmary, Newcastle upon Tyne, NE1 4LP, United Kingdom;
†Department of Medical Physics and Bioengineering, University College London, 11-20 Capper Street, London WC1E 6JA, United Kingdom;
and *Department of Electronics and Electrical Engineering, Keio University, 3-14-1, Hiyoshi, Kohoku-ku, Yokohama 223 Japan

Received October 7, 1997

Near-infrared (NIR) spectroscopy has been used in studies of the cerebral hemodynamic response to visual processing. In this paper, we present theoretical results from finite element and Monte Carlo modeling in order to help understand the contribution to the NIR signal from different parts of the head. The results from the models show that at the typical optode spacings used in these studies, an infrared spectroscopy measurement of *intensity* is sensitive to the outer 1–2 mm of the cortical gray matter and the partial optical path length in the gray matter is approximately 10 mm, compared with a total optical path length of 400 mm. When the NIR measurement is of *change in mean photon arrival time* (or *phase shift*), the signal comes from the upper 2–4 mm of the cortical surface and there is an increased lateral spread of the contributing tissue. We predict that for a 4-cm separation of input and detection optodes at 800 nm, a 1 μ M change in hemoglobin concentration in the cortex corresponds to an attenuation change of approximately 0.001 OD (optical density) or 1 ps mean time change. Movement of the brain caused by this increase in volume will cause an absorption change of approximately half this magnitude, but does not affect the photon arrival time at 4-cm spacing. A discrepancy between the predicted and the experimentally measured intensities may support the supposition that the NIR signal is actually very sensitive to changes occurring in the pial cerebral vessels lying on the brain surface. © 1998 Academic Press

INTRODUCTION

Near-infrared (NIR) spectroscopy can be used to noninvasively monitor variations in cerebral blood oxygenation by measuring changes in the attenuation of NIR light passing through tissue (Jöbsis, 1977; Ed-

wards *et al.*, 1988; Hampson and Piantadosi, 1988; Wyatt *et al.*, 1990; De Blasi *et al.*, 1993; Elwell *et al.*, 1994). To carry out a study, near-infrared light is transported to the head by optical fibers which are usually terminated with reflective prisms (henceforth called optodes) which direct the light into the tissues. Light is collected by a similar fiber arrangement and detected by a photomultiplier tube or photodiode. The separation between input and detection optodes is usually in the range 2–4 cm. Changes in optical attenuation are then measured at a number of wavelengths, and these can be related to changes in hemoglobin oxygenation and concentration using the known absorption spectra of the hemoglobin (Wray *et al.*, 1988). Measurements can also be made of time of flight of the light or the phase shift of intensity modulated light. A review of the different measurement types used in NIR spectroscopy can be found in Delpy and Cope (1997).

Recently, several authors (Hoshi and Tamura, 1993; Villringer *et al.*, 1993; Maki *et al.*, 1995; Meek *et al.*, 1995; Gratton *et al.*, 1995a) reported studies using NIR spectroscopy to investigate the response of the brain to visual or motor stimuli. For these studies, the optodes are placed on the scalp over the appropriate cortical area, a suitable stimulus protocol is followed, and changes in hemoglobin oxygenation and concentration are followed. One study (Gratton *et al.*, 1995b) also reported light-scattering changes in the tissues. Usually, the stimulus is repeated several times with a rest period between, and, if necessary, the measurements are averaged over the stimulus cycle.

At present, the interpretation of the measured attenuation is limited by incomplete knowledge of which regions in the brain are being sampled by the NIR light, although some attempts to define the region have been made by comparing NIRS data with that obtained from PET (Hoshi *et al.*, 1994; Hock *et al.*, 1997) and fMRI studies (Kleinschmidt *et al.*, 1996). Developments of mathematical models of light propagation are ongoing,

¹ To whom correspondence should be addressed.

and recent theoretical modeling (Okada *et al.*, 1997; Firbank *et al.*, 1996; Hielscher *et al.*, 1997) has indicated that the path taken by the light is greatly affected by the CSF, particularly in the adult head. The CSF is a clear fluid which cannot be modeled by simple diffusion theory approximations of light transport. Results from the more recent modeling, which can correctly incorporate the effects of the CSF, indicate that the light penetration in the adult brain may be limited to the outer cortical gray matter (Firbank *et al.*, 1996; Okada *et al.*, 1996, 1997).

The purpose of this investigation, therefore, was to model the distribution of light in the brain in a visual evoked-response study and to predict what proportion of the detected signal arises from cerebral tissue in order to help in the interpretation of experimentally measured changes in optical attenuation.

THEORETICAL BASIS OF OPTICAL SPECTROSCOPY *IN VIVO*

In a clear solution, light attenuation is linearly related to the compound concentration, its specific absorption coefficient, and the distance traveled through the solution. This is known as Beer's law. For a clear solution with absorption coefficient μ_a in a cuvette of thickness d , the attenuation A is given by

$$A = \ln(I_0/I) = \mu_a d, \quad (1)$$

where I_0 is the incident intensity and I the measured intensity. For a scattering medium, the distance the light travels is greater than the physical distance between the source and the detector, but it has been shown (Delpy *et al.*, 1988) that Eq. (1) can still be used to relate *changes* in absorption ($\Delta\mu_a$) to *changes* in attenuation (ΔA), provided that the mean distance, L , traveled by the light is known,

$$\Delta A = \ln(I_1/I_2) = \Delta\mu_a L, \quad (2)$$

where I_1 and I_2 are the intensities measured, and the mean distance

$$L = \beta d, \quad (3)$$

β being a numerical factor representing the increase in path traveled by the light due to multiple scattering.

Obviously, Eq. (2) can be rewritten in terms of the optical pathlength:

$$L = \frac{\Delta A}{\Delta\mu_a}. \quad (4)$$

This equation can be used to calculate the optical pathlength L in a homogeneous medium from the change in attenuation due to a small change in absorption coefficient. In the case of a heterogeneous medium, where the absorption can change differently in different regions, the partial path length can be defined for a change in region x :

$$L(x) = \frac{\Delta A}{\Delta\mu_a(x)}. \quad (5)$$

Since experimentally it is not possible to vary the absorption coefficient of tissues in a controlled manner, it is not possible to measure the partial path length of different regions of the head *in vivo*. Measurements in phantoms are possible, however, as are calculations of the partial path length from accurate mathematical models of light transport.

One implication of the above equation is that if a change in absorption (i.e., chromophore concentration) occurs in one region only, the change in μ_a (and hence concentration) can only be calculated if the partial path length in that region is known.

Photon Measurement Density Functions (PMDFs)

The PMDF describes how sensitive a measurement is to different points in the tissue. Two types of measurement are considered in this paper: simple attenuation changes, from which concentration changes can be derived as described above, and mean time measurements. The latter is a measurement of the average time taken by light to travel from the source to the detector optode. Obviously, this is equivalent to the mean distance traveled divided by the speed of light. Mean time can be measured either by timing ultrashort pulses of light as they pass through the tissue or by using amplitude-modulated light, in which case the phase shift of the detected light is measured. In tissue, mean time $\langle t \rangle$ and phase shift ϕ (in radians) are simply related by

$$\langle t \rangle = \frac{\phi}{2\pi f}, \quad (6)$$

provided that the modulation frequency, f , is less than 200 MHz (Arridge *et al.*, 1992).

The mean time (or phase shift) can be used as an *in vivo* measurement of total path length. Changes in μ_a and scattering coefficient (μ_s) will cause changes in it, as well as changing attenuation. Gratton *et al.* (1995b) reported fast changes (100–200 ms) in the phase shift during an evoked-response study which they claim are caused by changes in scattering as the neurons depolarize following the stimulation.

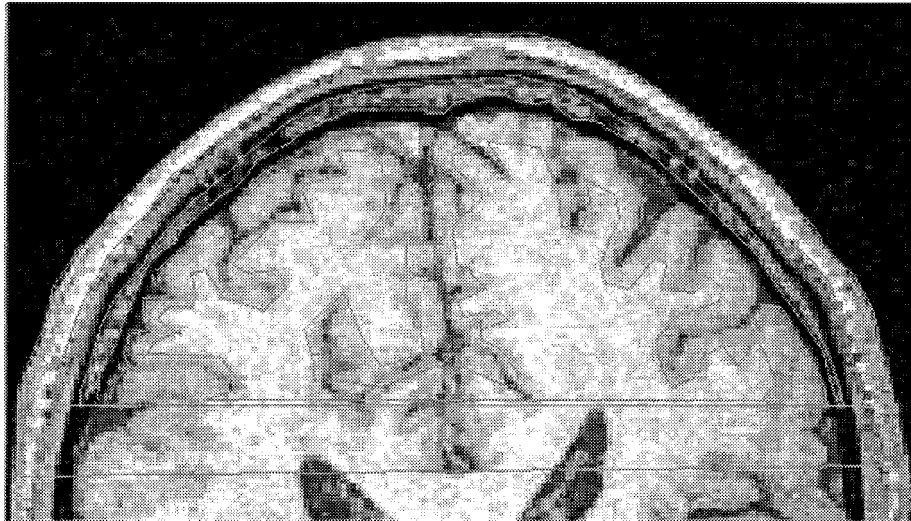


FIG. 1. A MRI scan with manually generated outlines.

The calculation of PMDFs, which has usually been done with diffusion theory, is discussed elsewhere (Arridge, 1995; Arridge and Schweiger, 1995), but a brief definition is as follows.

For intensity measurements, the PMDF $J(p, m, s)$ at position p in the tissue, for a source at s and measurement of change in fluence $\Delta\Gamma(m)$ at position m , is

$$J_{\Gamma}(p, m, s) = \frac{\Delta\Gamma(m)}{\Delta\mu_a(p)}, \quad (7)$$

$\Delta\mu_a(p)$ being the change in absorption coefficient at p .

Similarly, for mean time $\langle t \rangle$, the corresponding PMDF is

$$J_{\langle t \rangle}(p, m, s) = \frac{\Delta\langle t \rangle(m)}{\Delta\mu_a(p)}. \quad (8)$$

Note that the mean time PMDF can be either positive or negative, since an increase in absorption coefficient can cause either an increase or decrease in mean time depending upon the position of the change relative to the source and detector optodes.

Differential Mean Time Factor

To calculate the effect of absorption changes in a region on the mean time, we can define the differential mean time factor (DMTF) for region x in a similar fashion to Eq. (5):

$$\text{DMTF}(x) = \frac{\Delta\langle t \rangle}{\Delta\mu_a(x)}. \quad (9)$$

TECHNIQUES

A MRI scan of one of the authors' heads was taken and an axial slice through the region of the visual cortex selected. This image was used to generate outlines (Fig. 1) of the gray matter, white matter, CSF, and extra cerebral tissue (skull, skin). These outlines were used to generate a finite element mesh (see Fig. 2). The approximate radii of the tissue types were also measured and used in a separate cylindrical model of the tissues. The dimensions and tissue optical properties (absorption coefficient μ_a and transport scattering coefficient μ'_s) are shown in Table 1.

The optical properties are typical of those quoted in the literature (Firbank *et al.*, 1993; van der Zee *et al.*, 1993; Cheong, 1995) at 800 nm. Oxygenated and deoxygenated hemoglobin have an isobestic point at 798 nm, with an absorption coefficient of $0.2 \text{ mm}^{-1} \text{ mM}$ (Matcher *et al.*, 1995). All absorption and scattering coefficient are in base e .

Since diffusion theory is only valid in scattering regions, a hybrid diffusion/radiosity model was used to calculate light transport in the head. In this scheme, which has been specifically developed to cope with tissues containing clear regions (Firbank *et al.*, 1996), a 2D finite element model (FEM) solution of the diffusion equation (Arridge *et al.*, 1993) is used to calculate light transport in the scattering regions, while in the nonscattering regions of the CSF (the blank section in the middle of the mesh in Fig. 2), radiosity light tracing is employed. This hybrid scheme has been validated against both experimental measurements in phantoms and a Monte Carlo model (Firbank *et al.*, 1996).

In addition, we performed a Monte Carlo simulation (Hiraoka *et al.*, 1993) of a concentric cylinder with

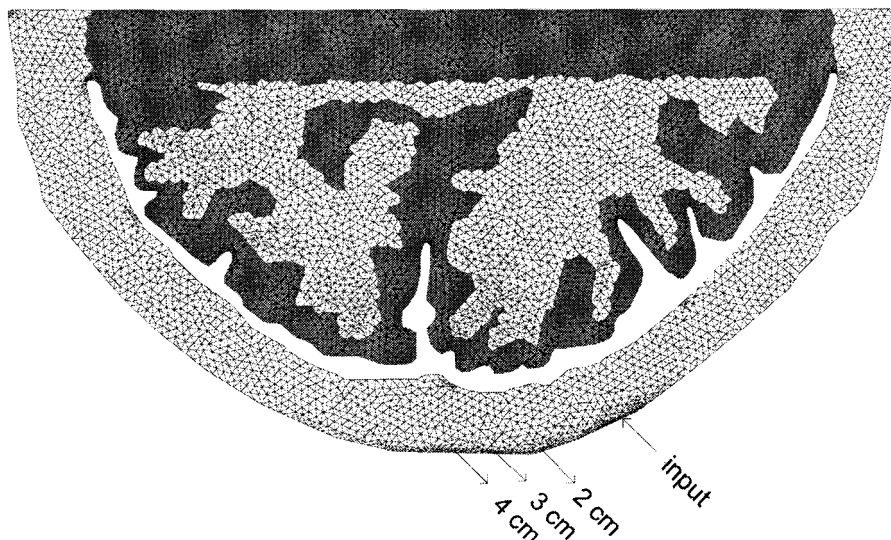


FIG. 2. Finite element mesh generated from Fig. 1.

properties as shown in Table 1, using 5 million input photons. This was a 3D simulation. FEM/radiosity calculations were also performed for a 2D cylindrical geometry.

The simplified cylindrical geometry was used in order to investigate the effect of changing the thickness of the CSF, since it is easier to define a thickness change for a uniform layer (in a previous study, we have shown that the presence of the sulci have little effect upon the thickness of the brain tissue contributing to the NIRS signal) (Okada *et al.*, 1997). The FEM model based upon the MRI data, however, allowed qualitative analysis of the effect of the nonuniformity of the gray matter surface. The 3D Monte Carlo cylinder model was run to investigate the spread of light perpendicular to the measurement plane, since this is not possible to do in a 2D model (which our finite element model is currently restricted to because of the computation time required).

PMDFs were generated with source/detector separations of 2, 3, and 4 cm which are typical of the values used in the published evoked-response studies. The input position for the light in the MRI generated geometry is shown in Fig. 2. This was chosen to be approximately over the visual cortex while avoiding the sagittal sinus. Data for the surface fluence and mean time were calculated at all detector positions.

TABLE 1

Tissue	Radius (mm)	μ_a (mm^{-1})	μ'_s (mm^{-1})
White matter	68.5	0.005	6.0
Gray matter	75.5	0.025	2.5
CSF	79.0	0.003	0.001
Skin/skull	92.0	0.01	2.0

RESULTS

Figure 3 shows the PMDFs for measurements of mean time and intensity for the FEM calculations on the head. These show that for a measurement of *intensity*, the region of the brain which is interrogated is limited to the cortical gray matter immediately below and between the optodes and that this region is sampled approximately uniformly. For a measurement of *mean time* (or *phase* if using an intensity modulated spectrometer) a slightly greater region is sampled in terms of both depth and lateral spread. The depth of gray matter sampled does not increase substantially with increased optode spacing. Figures 4a and 4b show profiles of the PMDFs in the brain tissue halfway between the optodes and perpendicular to them (in the 2D plane) for source/detector spacings of 2, 3, and 4 cm. The profiles have been normalized by dividing each of them by the received signal at the appropriate spacing. The contribution of the tissue to the detected signal falls exponentially with distance into the gray matter; the $1/e$ penetration depth for the intensity PMDF in the gray matter can be calculated as 1.5 mm and for the mean time as 2.4 mm.

Figure 5a shows the optical path lengths in each of the tissue types as a function of optode spacing. This is proportional to the attenuation change caused by a variation in absorption within that region. A $1 \mu\text{M}$ increase in blood concentration in the skin will hence give rise to a change in attenuation approximately 20 times bigger than a $1 \mu\text{M}$ change in the gray matter. The partial path length through the white matter is less than 0.5 mm and is effectively zero on this scale, and hence changes in blood concentrations solely occurring there will not be seen.

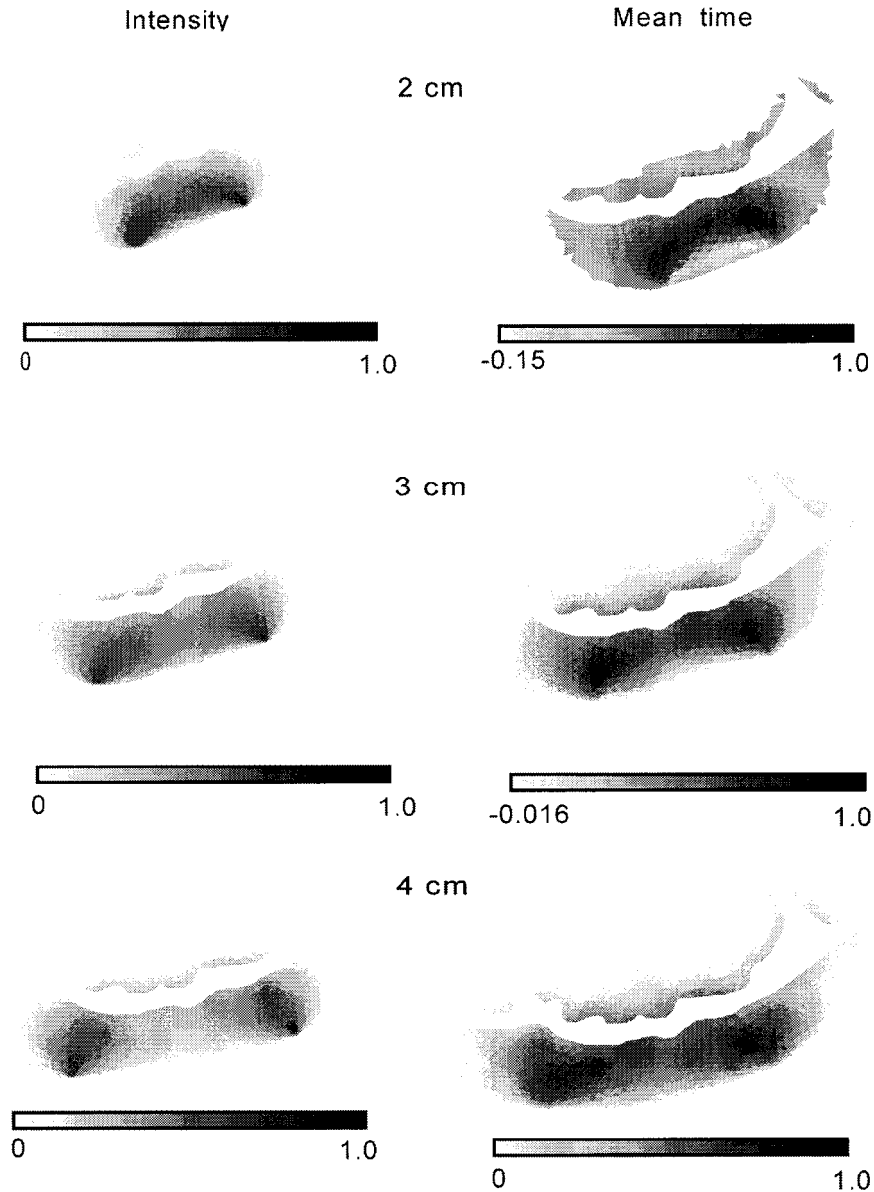


FIG. 3. Intensity and mean time PMDFs for 2-, 3-, and 4-cm optode separation. For the intensity PMDF, dark color indicates an increase in attenuation with increase in μ_a . For the mean time PMDF, dark color indicates a decrease in mean time with increase in μ_a and light color an increase in mean time.

Figure 5b shows a similar graph for the mean time, the y axis showing the change in mean time for a change in absorption coefficient. The mean time measurement is approximately twice as sensitive to changes occurring in the brain than the intensity measurement, although it still is a factor of 10 less than the surface regions.

Information about the spread of photons perpendicular to the source/detector plane was gained from the 3D concentric cylinder Monte Carlo model by recording the position of all detected photons as they passed through the surface of the gray matter. The resulting intensity

PMDFs are shown in Fig. 6. Figure 7 shows the profile through the PMDFs along the axis indicated by the dotted line normalized by the total detected intensity. As can be seen, the light probes an area of brain approximately 1 cm on either side of the source/detector plane. This vertical spread does not change significantly with source/detector spacing. It is worth noting that the use of a cylindrical as opposed to a spherical 3D model would, if anything, slightly overestimate the vertical spread to be expected, so the values presented here probably represent a maximum extent to the sampled tissue volume (Okada *et al.*, 1996, 1997).

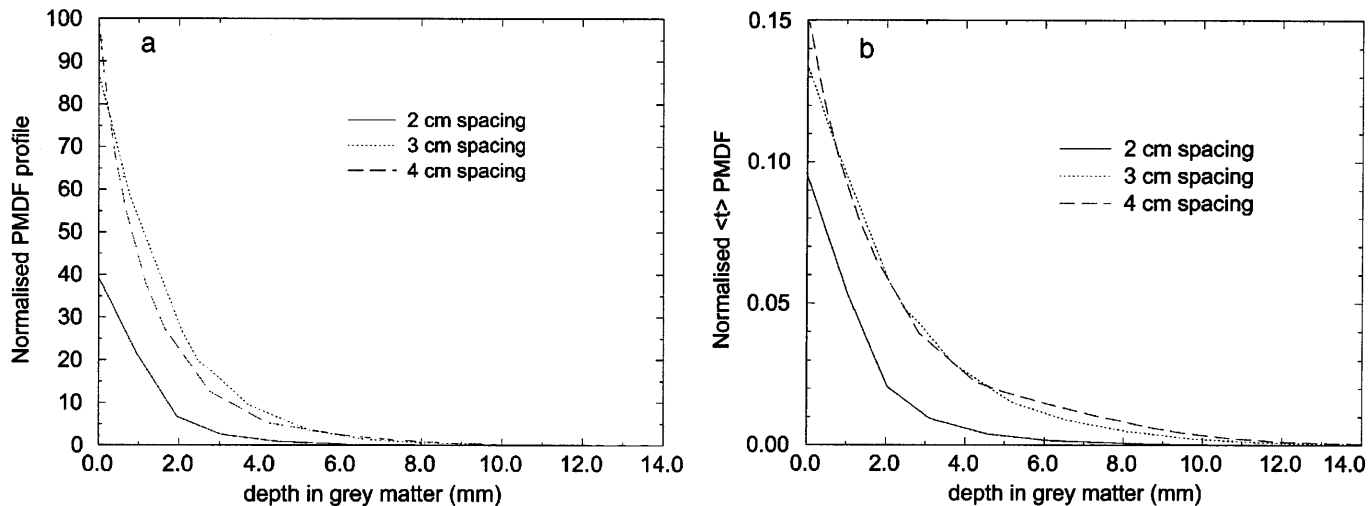


FIG. 4. Profile through (a) intensity and (b) mean time PMDFs in gray matter for 2-, 3-, and 4-cm optode separation for the FEM/radiosity calculation on the MRI-generated mesh.

Effect of Brain Movement

In NIRS studies, optical changes can be observed in synchrony with both the heart and the respiratory rates, and these need to be filtered out in measuring the small evoked-response signal (Gratton and Corballis, 1995). These signals have usually been assumed to be due to changes in blood flow/volume that occur with each heart beat or respiration (Elwell *et al.*, 1994), but it is also possible that they can arise due to movements of the brain surface or from pial cerebral vessels lying on the brain surface. The brain is not fixed inside the skull and can move or expand to a limited degree. The pulsatile nature of the blood flow causes the brain to

throb with the heart beat. This has been observed in patients undergoing brain surgery, although in NIR studies, of course, the skull is not opened, and the brain has less room for movement.

Changes in the blood volume of the brain (as part of an evoked response) will also lead to a change in brain volume and will cause it to expand or shrink, displacing CSF. Both the absorption and the volume change may alter the light distribution in the head, resulting in an optically observable signal. We have applied our previously described modeling to determine the relative contributions of movement and absorption variation to the NIRS signal.

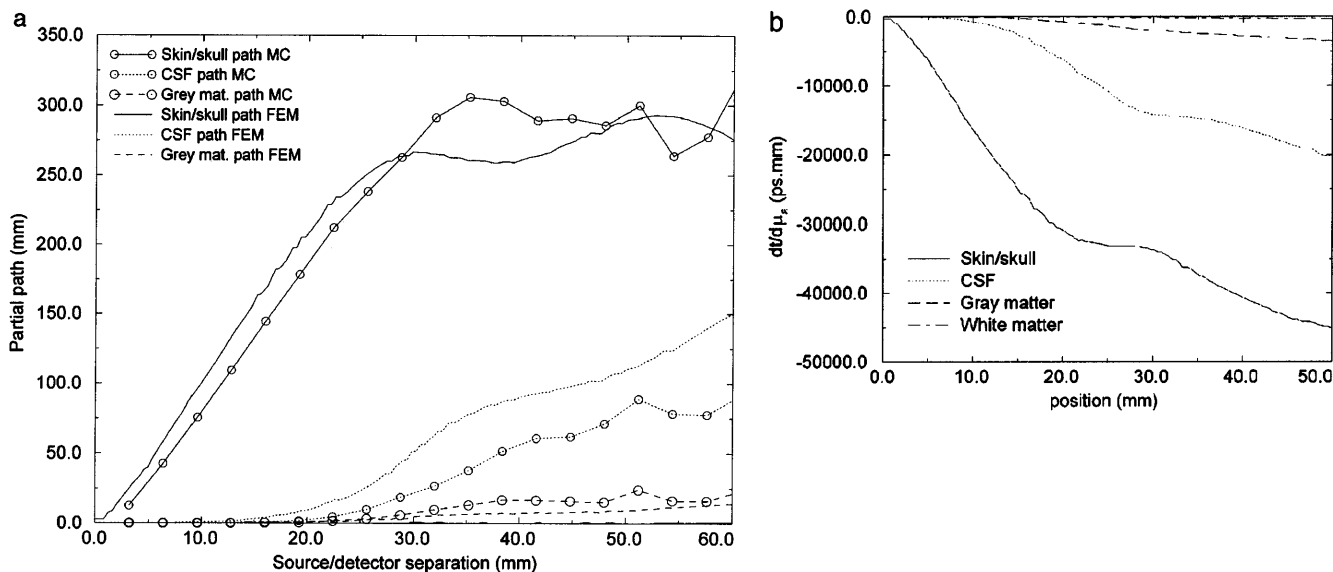


FIG. 5. (a) Partial path lengths through skin/skull, CSF, and gray matter for FEM/radiosity calculation on the MRI-generated mesh and Monte Carlo modeling of the 3D cylinder and (b) differential mean time factor for different regions for FEM/radiosity calculation on the MRI-generated mesh.

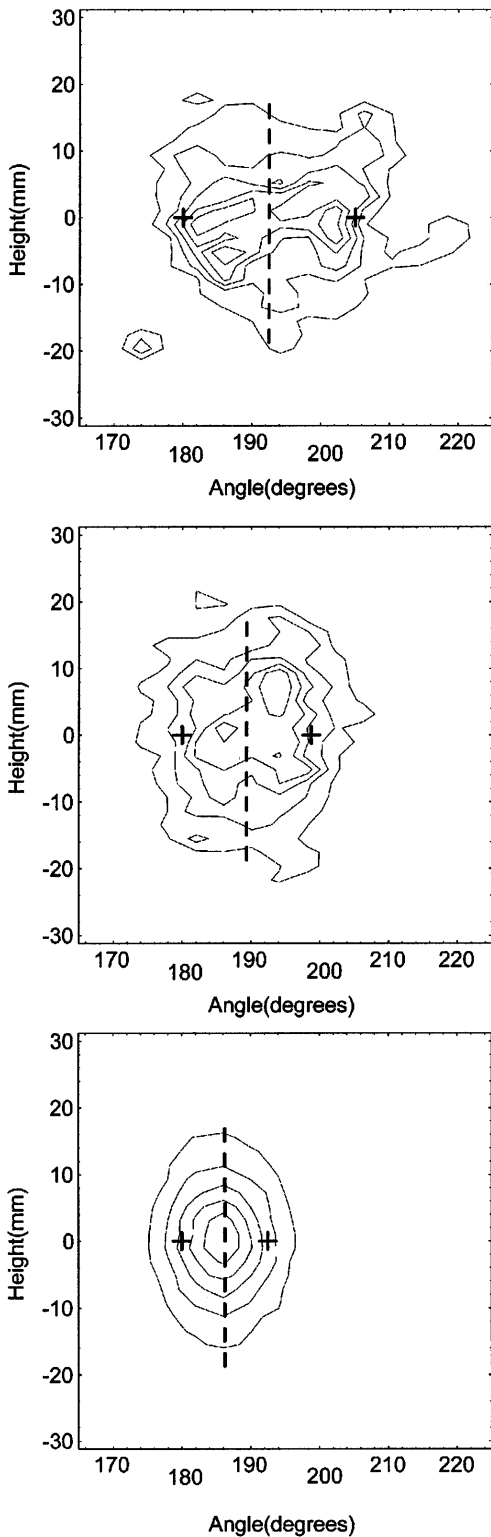


FIG. 6. Monte Carlo-generated intensity PMDFs for the gray matter/CSF interface, showing the vertical spread of the light on the gray matter surface. PMDFs are shown for light detected at 2-, 3-, and 4-cm separation. The positions of the optodes are shown with a cross. The dotted line shows the direction across which the profiles were generated (see Fig. 7).

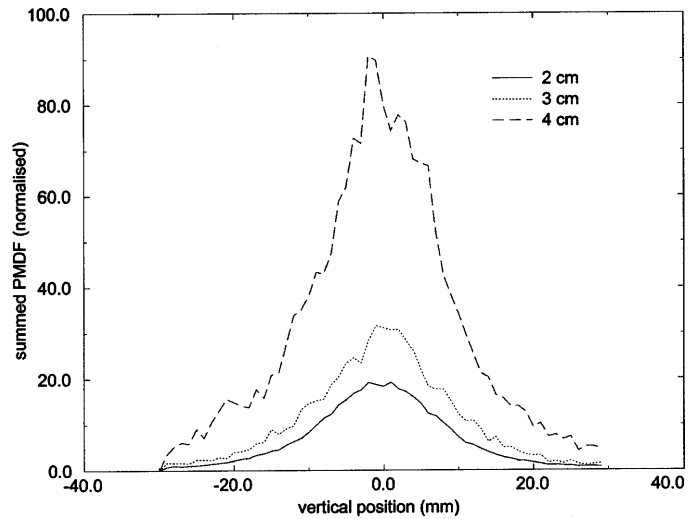


FIG. 7. Profile of detected photons as they cross the gray matter boundary for 2-, 3-, and 4-cm source/detector spacing.

Greitz *et al.* (1992) reported pulsatile brain movement using magnetic resonance phase imaging in adult volunteers. This movement was greatest around the base of the brain (0.1 mm displacement and velocities of up to 2 mm/s). The magnitude of the motion decreased toward the periphery of the brain, however, and was less than 0.01 mm at the brain surface.

Figure 8 shows the calculated change in attenuation and mean time for a decrease of 0.1 mm of the CSF thickness in the simplified cylindrical model (i.e., the inner radius of the CSF changes from 75.5 to 75.6 mm, with all other parameters remaining constant).

When the blood volume in the brain increases, the attenuation will change for two reasons: (a) because the blood content has increased, causing higher absorption, and (b) because the brain will expand slightly, changing the distribution of light in the head. Figure 9 shows a

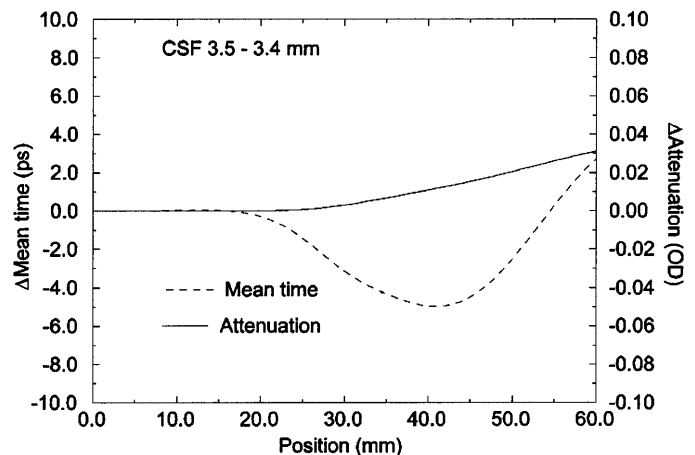


FIG. 8. Change in attenuation and mean time for CSF thickness decreasing from 3.5 to 3.4 mm (in 2D cylinder FEM/radiosity).

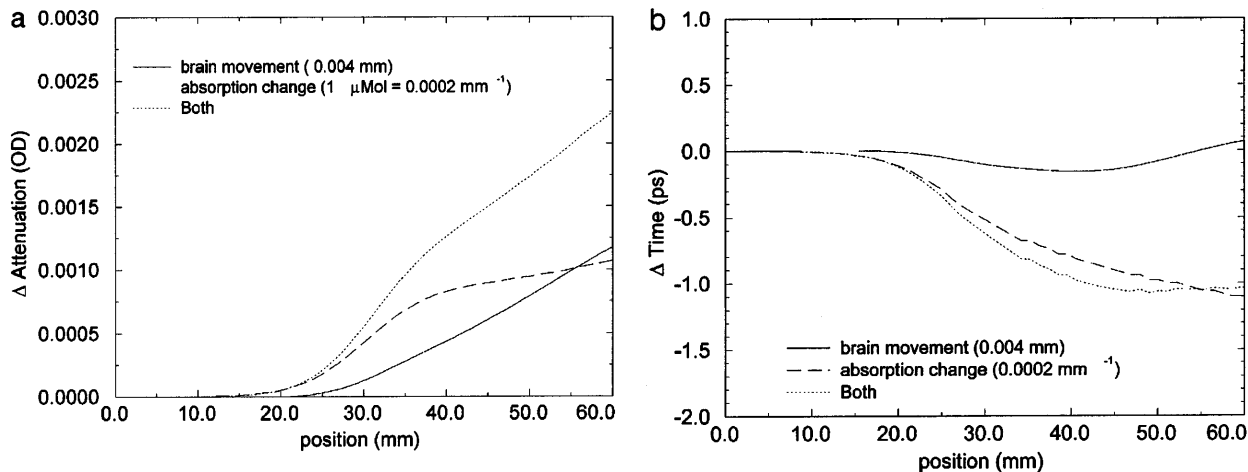


FIG. 9. Comparison of signal change for (a) attenuation and (b) mean time caused by an absorption increase with that caused by brain expansion due to increased blood volume (from 2D cylinder FEM/radiosity calculation).

comparison of these two effects, i.e., an increased absorption, but constant geometry, and an increased brain volume at constant absorption. The data are calculated for a $1 \mu\text{M}$ change of hemoglobin concentration in the gray matter. The gray matter thickness is 7 mm and the brain blood volume is approximately 5% with a typical hemoglobin concentration of $84 \mu\text{M}$ (Sakai *et al.*, 1985), so a $1 \mu\text{M}$ increase is equivalent to $5 \times 1/84 = 0.06\%$ increase in volume and so assuming that the brain swells outward only and that the brain hematocrit stays constant, this is equivalent to an increase of 0.004 mm in thickness.

IMPLICATIONS

When used on the scalp surface, NIR spectroscopy can pick up changes in hemoglobin concentration on the cortical surface. The signal is probably limited to changes in hemodynamics occurring in the top 2–3 mm of the cortex. The area of the brain surface which contributes to the signal is approximately as wide as the optode spacing and extends laterally 1 cm either side perpendicular to the optode position. In NIR spectroscopy, the calculated quantity ΔCL is a product of the changes in concentration and optical pathlength. To derive absolute changes in concentration, the optical path length must be known. If the concentration changes are limited to one region only, the partial path length in that region must be known to calculate the change in concentration correctly. In the case of evoked response studies, the hemoglobin concentration changes are assumed to occur in the brain only. Although the PMDFs are weighted toward surface tissues, this does not necessarily mean that NIRS signal comes mainly from the surface. This is because in evoked-response studies, we are measuring *changes* in signal, and if the

only change in hemodynamics occurs in the brain, then that is what will be detected. The technique is, however, more sensitive to changes occurring in the skin and skull than in the brain.

While the exact dependence of the NIR signal contribution in an individual study will depend upon the geometry and the exact optical properties, in our theoretical model, we found that a $1 \mu\text{M}$ change in blood concentration will give rise to approximately 0.001 OD change in attenuation at 4-cm spacing and approximately 1-ps change in mean time. Typical instrumental noise at 3-cm spacing in tissue is 0.001 OD for attenuation and 0.1° in phase (equal to 1.4 ps at 200 MHz). This typically gets a factor of 3 worse for every centimeter increase in optode spacing and is essentially limited by the detected intensity and the quantum efficiency of the detecting device. The signal can of course be improved by averaging and performing several studies on the same volunteer.

It is interesting to note that, although experimentally the NIRS signal changes measured over the visual cortex vary considerably in magnitude from subject to subject, the average level of intensity change (Meek *et al.*, 1995) and phase change (Gratton *et al.*, 1995a) observed is approximately five times greater than that predicted from this simple modeling in which the hemoglobin changes are assumed to occur only in the brain parenchyma. We have previously speculated (Okada *et al.*, 1997, 1998) that the considerable time spent by the light in the clear CSF would lead to it contributing significantly to the NIRS signal were an absorption change to occur within it. In reality, the CSF layer comprises the subarachnoid space which includes pial cerebral vessels lying on the brain surface. Any small change in the hemoglobin concentration, oxygenation, or size of these vessels as a result of an evoked

response is likely therefore to be a major contributor to the experimentally observed signal. The current hybrid diffusion/radiosity model cannot deal with this geometry, but work is under way to modify it to enable the effect of discrete absorbers within the clear layer to be modeled.

ACKNOWLEDGMENTS

The authors thank the EPSRC (Grant GR/K07386) and Hamamatsu Photonics KK for financial support. The MRI scan was taken at the Institute of Neurology, Queen's Square, London.

REFERENCES

- Arridge, S. R. 1995. Photon measurement density functions. Part I: Analytical forms. *Appl. Opt.* **34**:7395–7409.
- Arridge, S. R., and Schweiger, M. 1995. Photon measurement density functions. Part II: Finite element method calculations. *Appl. Opt.* **34**:8026–8037.
- Arridge, S. R., Schweiger, M., Hiraoka, M., and Delpy, D. T. 1993. A finite element approach for modelling photon transport in tissue. *Med. Phys.* **20**(2):299–309.
- Arridge, S. R., Cope, M., and Delpy, D. T. 1992. The theoretical basis for the determination of optical pathlengths in tissue: Temporal and frequency analysis. *Phys. Med. Biol.* **37**:1531–1560.
- Cheong, W.-F. 1995. Summary of optical properties. In *Optical-Thermal Response of Laser-Irradiated Tissue* (A. J. Welch and M. J. C. van Gemert, Eds.), pp. 275–303. Plenum, New York.
- De Blasi, R. A., Cope, M., Elwell, C. E., Safoue, F., and Ferrari, M. 1993. Noninvasive measurement of human forearm oxygen consumption by near infrared spectroscopy. *J. Appl. Physiol.* **67**:20–25.
- Delpy, D. T., Cope, M., van der Zee, P., Arridge, S. R., Wray, S., and Wyatt, J. S. 1988. Estimation of optical pathlength through tissue from direct time of flight measurements. *Phys. Med. Biol.* **33**:1433–1442.
- Delpy, D. T., and Cope, M. 1997. Quantification in tissue near infrared spectroscopy. *Philos. Trans. R. Soc. London B* **352**:649–659.
- Edwards, A. D., Wyatt, J. S., Richardson, C. E., Delpy, D. T., Cope, M., and Reynolds, E. O. R. 1988. Cotside measurement of cerebral blood flow in ill newborn infants by near infrared spectroscopy. *Lancet* **2**:770–771.
- Elwell, C. E., Cope, M., Edwards, A. D., Wyatt, J. S., Delpy, D. T., and Reynolds, E. O. R. 1994. Quantification of adult cerebral haemodynamics by near-infrared spectroscopy. *J. Appl. Physiol.* **77**:2753–2760.
- Firbank, M., Arridge, S. R., Schweiger, M., and Delpy, D. T. 1996. An investigation of light transport through scattering bodies with non-scattering regions. *Phys. Med. Biol.* **41**:767–783.
- Firbank, M., Hiraoka, M., Essenpreis, M., and Delpy, D. T. 1993. Measurement of the optical properties of skull in the wavelength range 650–950 nm. *Phys. Med. Biol.* **38**:503–510.
- Gratton, G., Corballis, P. M. 1995. Removing the heart from the brain: Compensation for the pulsatile artifact in the photon migration signal. *Psychophysiology* **32**:292–299.
- Gratton, G., Corballis, P., Cho, E., Fabiani, M., and Hood, D. C. 1995a. Shades of gray matter: Noninvasive optical images of human brain responses during visual stimulation. *Psychophysiol.* **32**:505–509.
- Gratton, G., Fabiani, M., Friedman, D., Franceschini, M. A., Fantini, S., Corballis, P., and Gratton, E. 1995b. Rapid changes of optical parameters in the human brain during a tapping task. *J. Cognit. Neurosci.* **7**(4):446–456.
- Greitz, D., Wirestam, R., Franck, A., Nordell, B., Thomsen, C., and Ståhlberg, 1992. Pulsatile brain movement and associated hydrodynamics studied by magnetic resonance phase imaging: The Monro-Kellie doctrine revisited. *Neuroradiology* **34**:370–380.
- Hielscher, A. H., Alcouffe, R. E., and Barbour, R. L. 1997. Transport and diffusion calculations on MRI generated data. *Proc. SPIE* **2979**:500–508.
- Hiraoka, M., Firbank, M., Essenpreis, M., Cope, M., Arridge, S. R., van der Zee, P., and Delpy, D. T. 1993. A Monte Carlo investigation of optical pathlength in inhomogeneous tissue and its application to near infrared spectroscopy. *Phys. Med. Biol.* **38**:1859–1876.
- Hock, C., Villringer, K., MullerSpahn, F., Wenzel, R., Heekeren, H., SchuhHofer, S., Hofmann, M., Minoshima, S., Schwaiger, M., Dirnagl, U., and Villringer, A. 1997. Decrease in parietal cerebral hemoglobin oxygenation during performance of a verbal fluency task in patients with Alzheimer's disease monitored by means of near-infrared spectroscopy (NIRS)—Correlation with simultaneous rCBF—PET measurements. *Brain Res.* **755**:293–303.
- Hoshi, Y., and Tamura, M. 1993. Detection of dynamic changes in cerebral oxygenation coupled to neuronal function during mental work in man. *Neurosci. Lett.* **150**:5–8.
- Hoshi, Y., Onoe, H., Watanabe, Y., Andersson, J., Bergström, Lilja, A., Langstöm, and Tamura, M. 1994. Non synchronous behaviour of neuronal activity, oxidative metabolism and blood supply during mental tasks in man. *Neurosci. Lett.* **172**:129–133.
- Jöbsis, F. F. 1977. Noninvasive infrared monitoring of cerebral and myocardial oxygen sufficiency and circulatory parameters. *Science* **198**:1264–1267.
- Kleinschmidt, A., Obrig, H., Requardt, M., Merboldt, K.-D., Dirnagl, U., Villringer, A., and Frahm, J. 1996. Simultaneous recording of cerebral blood oxygenation changes during human brain activation by magnetic resonance imaging and near infrared spectroscopy. *J. Cereb. Blood Flow Metab.* **16**:817–826.
- Maki, A., Yamashita, Y., Ito, Y., Watanabe, E., Mayanagi, Y., and Koizumi, H. 1995. Spatial and temporal analysis of human motor activity using noninvasive NIR topography. *Med. Phys.* **22**(12):1997–2005.
- Matcher, S. J., Elwell, C. E., Cooper, C. E., Cope, M., and Delpy, D. T. 1995. Performance comparison of several published tissue near-infrared spectroscopy algorithms. *Anal. Biochem.* **227**:54–68.
- Meek, J. H., Elwell, C. E., Khan, M. J., Romata, J., Wyatt, J. S., Delpy, D. T., and Zeki, S. 1995. Regional changes in cerebral haemodynamics as a result of a visual stimulus measured by near infrared spectroscopy. *Proc. R. Soc. London B* **261**:351–356.
- Okada, E., and Delpy, D. T. 1996. The effect of overlying tissue on NIR light propagation in neonatal brain. *OSA TOPS Adv. Opt. Imaging Photon Migrat.* **2**:338–343.
- Okada, E., Firbank, M., Schweiger, M., Arridge, S. R., Cope, M., and Delpy, D. T. 1997. Theoretical and experimental investigation of near infrared light propagation in a model of the adult head. *Appl. Opt.* **36**:21–31.
- Okada, E., Tanigawa, Y., Yamada, Y., Firbank, M., and Delpy, D. T. 1998. Investigation of the direct and indirect signal contribution of brain haematoma in near infrared spectroscopy. *OSA TOPS Adv. Opt. Imaging Photon Migrat.*, in press.
- Sakai, F., Nakazawa, K., Tazaki, Y., Ishii, K., Hino, H., Igarashi, H., and Kanda, T. 1985. Regional cerebral blood volume and hematocrit measured in normal human volunteers by single photon emission computed tomography. *J. Cereb. Blood Flow Metab.* **5**:207–213.
- van der Zee, P., Essenpreis, M., and Delpy, D. T. 1993. Optical properties of brain tissue. *Proc. SPIE* **1888**:454–465.

- Villringer, A., Planck, J., Hock, C., Schleinkofer, L., and Dirnagl, U. 1993. Near infrared spectroscopy (NIRS) a new tool to study hemodynamic changes during activation of brain function in human adults. *Neurosci. Lett.* **154**:101–104.
- Wray, S., Cope, M., Delpy, D. T., Wyatt, J. S., and Reynolds, E. O. R. 1988. Characterization of the near infrared absorption spectra of cytochrome aa3 and haemoglobin for the non invasive monitoring of cerebral oxygenation. *Biochim. Biophys. Acta* **933**:184–192.
- Wyatt, J. S., Cope, M., Delpy, D. T., Richardson, C. E., Edwards, A. D., Wray, S., and Reynolds, E. O. R. 1990. Quantitation of cerebral blood volume in human infants by near infrared spectroscopy. *J. Appl. Physiol.* **68**:1086–1091.